Science of the Total Environment 1031 (2026) 181809

Contents lists available at ScienceDirect

Science of the Total Environment

journal homepage: www.elsevier.com/locate/scitotenv

Global oxygen distributions at the Earth's surface

Andrew S. Kowalski [a,b,*], Matilde García-Valdecasas Ojeda [a,b]

[a] Departamento de Física Aplicada, Universidad de Granada, Granada, Spain
[b] Instituto Interuniversitario de Investigación del Sistema Tierra en Andalucía (IISTA), Granada, Spain

HIGHLIGHTS

- Humidity, not biology, controls surface oxygen gradients.
- Dry-air oxygen data overestimates abundance by up to 10,000 ppm in tropics.
- Oxygen's distributions, transport mechanisms, and ocean forcing are elucidated.

GRAPHICAL ABSTRACT

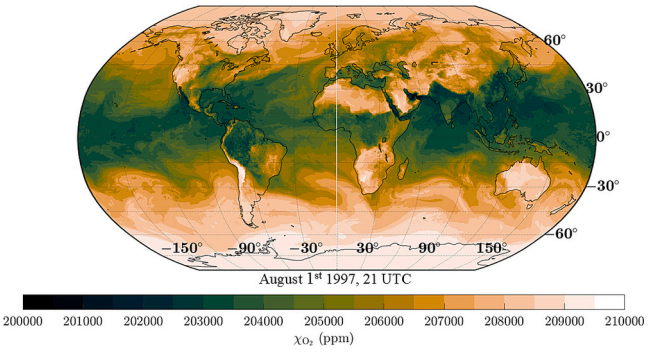

ARTICLE INFO

Keywords:
Oxygen
Humidity
Partial pressure
Non-diffusive transport

ABSTRACT

Available oxygen (O_2), described by its partial pressure (p_{O_2}), governs key aerobic processes like dissolution, respiration, and oxidation. It makes up a practically constant fraction of the partial pressure of dry air (p_d), which declines at constant pressure (p) with rising water vapor pressure (e) according to Dalton's law ($p = p_d + e$). Since sea level p does not increase equatorward away from temperate zones, tropical humidity—with e reaching several percent of p—suppresses both p_d and p_{O_2} by equal proportions. Oxygen's molar fraction (χ_{O_2}) reflects this, dropping by thousands of ppm in the tropics, unlike the humidity-invariant dry-air fraction ($\chi_{O_2,d}$), which varies inversely with carbon dioxide over mere dozens of ppm. Past O_2 studies eliminated water vapor and analyzed dry air expressing $\chi_{O_2,d}$, which was useful in constraining the carbon cycle but misrepresented O_2 abundances and gradients. Using ERA5 reanalysis data, we estimate molar fractions of dry air (χ_d) to map global χ_{O_2}, revealing strong meridional gradients from the highly aerobic winter pole to the relatively hypoxic tropics. Reckoning with humidity's control over p_d and χ_d clarifies key features of atmospheric O_2 cycling such as cross-equatorial exchanges, air-sea fluxes, and the physical mechanisms of gas transport. This challenges transport models based exclusively on diffusion and highlights the hydrological cycle's role in propelling air away from water vapor sources, significantly conveying not only O_2, but also greenhouse gases like methane and nitrous oxide.

* Corresponding author at: Departamento de Física Aplicada, Universidad de Granada, Avenida Fuente nueva S/N, 18071, Granada, Spain.
E-mail addresses: andyk@ugr.es (A.S. Kowalski), mgvaldecasas@ugr.es (M. García-Valdecasas Ojeda).

https://doi.org/10.1016/j.scitotenv.2026.181809
Received 24 November 2025; Received in revised form 14 April 2026; Accepted 14 April 2026
Available online 21 April 2026

1. Introduction

Interest in global oxygen (O_2) distributions extends beyond their role in constraining the carbon cycle, wherein O_2's *dry-air* fraction ($\chi_{O_2,d}$) and that of carbon dioxide (CO_2) vary inversely through O_2:C exchange stoichiometry (Keeling and Shertz, 1992). Many aerobic processes instead depend on O_2's partial pressure (p_{O_2}), which tracks $\chi_{O_2,d}$ only in very dry conditions. Via Henry's law, p_{O_2} sets the upper boundary for oceanic O_2, governing air–sea exchange and influencing the meridional transport of dissolved O_2 by ocean circulation (Najjar and Keeling, 2000; Portela et al., 2024). Oxygen availability also regulates oxidation processes such as wildfire propagation by affecting ignition probability (Watson et al., 1978). Because hypoxia suppresses organic matter mineralization (Keiluweit et al., 2016), humidity-suppressed p_{O_2} can also limit soil respiration, a major flux in the global C cycle (Raich and Schlesinger, 1992).

Because atmospheric pressure (p) at sea level varies little horizontally and over time, a simple fraction often serves as a reasonable proxy for O_2 availability. Thus, disciplines ranging from human health (Spelce et al., 2016) to geoscience (Keeling and Shertz, 1992) commonly describe O_2 levels as near 21%. But this raises an essential question: "Twenty-one percent of what?"

This question is relevant because O_2 concentrations commonly are reported on a dry-air basis, excluding water vapor. As a result, the stated O_2 content refers to "twenty-one percent of dry air." This convention is widely used when expressing fractions of any gas (Wallace and Hobbs, 2006; Tohjima et al., 2005), primarily for practical reasons. For example, metabolic processes assessed by measuring CO_2 concentrations can be biased when not accounting for humidity's diluting effect—using dry-air fractions automatically corrects for this (Pérez-Priego et al., 2015). Also, air samples are typically dried before compositional analysis, eliminating water vapor and often with no accounting of air's discarded fraction (Steele et al., 1987; Prinn et al., 1990; Keeling and Shertz, 1992; Novelli et al., 1999; Khalil et al., 2002; Tohjima et al., 2005); this standard practice prevents condensation damaging instruments, but inopportunely obscures the impact of humidity on gas abundances (Kowalski et al., 2025).

Traditional studies of atmospheric O_2 availability have focused on the dry-air fraction, particularly the O_2/N_2 ratio. This metric varies mainly with sources and sinks of O_2 and is unaffected by dilution by water vapor or CO_2, making it valuable for constraining the carbon cycle. However, because it neglects humidity—the primary control on air's O_2 content and its gradients—it can misrepresent the physical mechanisms governing O_2 transport.

Here we show that the omission of water vapor in analyses may have contributed to a substantial overestimation of air's O_2 content and considerable underestimation of its variability. Using pressure and humidity data from the ERA5 reanalysis, we compute the molar fraction of dry air (χ_d), which varies significantly and inversely with that of water vapor (χ_v). Since O_2's molar fraction (χ_{O_2}) is a quite constant proportion of χ_d, it follows similar patterns. We map χ_{O_2} globally to reveal its spatial distributions, including seasonal and interannual variability. Compared to previous estimates that neglected humidity, our approach reduces uncertainty in air's O_2 content by at least an order of magnitude. These revised patterns offer a new perspective on O_2 availability at the surface and provide insight into the relative roles of diffusive and non-diffusive transport mechanisms in the atmosphere.

2. Theory

Dalton's law defines p as the sum of the partial pressures of dry air (p_d) and water vapor (e), or

$$p = p_d + e. \tag{1}$$

Crucially, sea-level p does not rise in step with e along the gradient from temperate regions to the sultry tropics where e reaches several percent of p; therefore, p_d must decline. In fact, approaching the tropics p remains quite constant (isobaric) or even drops slightly to equatorial lows, confirming that tropical humidity suppresses p_d and thus p_{O_2}. This shows that relying on $\chi_{O_2,d}$ has caused air's O_2 content to be overestimated, and exposes the mistaken assumption that air's O_2 fraction is practically constant. Rather, humidity-controlled χ_{O_2} contrasts the relatively hypoxic tropics with the highly aerobic conditions that prevail in polar winters, and better portrays O_2 abundance.

Atmospheric composition varies primarily as a function of humidity. Water vapor is the only air constituent whose atmospheric fluctuations directly and significantly modify the molar fractions of other gases. Dividing Eq. (1) by p yields the fractional version of Dalton's law

$$100\% = \chi_d + \chi_v. \tag{2}$$

This equivalently describes how humidification suppresses dry-air availability, particularly in an isobaric context. Negligible in polar winters, χ_v generally exceeds 3% (30,000 ppm) near tropical surfaces (Famiglietti et al., 2018), and can reach extremes of 5% (Wallace and Hobbs, 2006). Humidity's seasonal variation is of a similar magnitude in certain climates (Dai, 2006). Since χ_d varies in perfect anti-correlation with χ_v over tens of thousands of ppm, Eq. (2) explains how humidity chiefly determines the concentrations of certain gases.

Water vapor overwhelmingly dominates air's sources and sinks, shaping the distributions, gradients, and transport of other gases through both diffusive and non-diffusive mechanisms (Kowalski et al., 2025). Although distinct, these mechanisms are coupled because evapotranspiration simultaneously dilutes and displaces dry-air constituents, activating offsetting transport processes (Kowalski et al., 2021). Dry-air components can therefore be grouped (Fig. 1) by the sensitivity of their mole-fraction gradients to humidity-driven variations in χ_d, which also reflects the importance of opposing, non-diffusive transport due to mass flow. Because source–sink flows originate at sources and terminate at sinks (Owen et al., 1985), and water vapor dominates those of air, water vapor dynamics ultimately governs both χ_d gradients and air's source–sink flows—the respective drivers of diffusive and non-diffusive transport.

Dry-air component gases differ according to how significantly their net transport is influenced by water vapor dynamics. Extremely reactive and scarce Category I gases—on the left of the spectrum in Fig. 1—are typified by ozone (O_3), whose net transport responds negligibly to humidity fluctuations. Chemical reactions involving O_3 predominantly determine its partial pressure (p_{O_3}), which spans orders of magnitude at the surface (Robeson and Steyn, 1990). As a result, its dry-air fraction

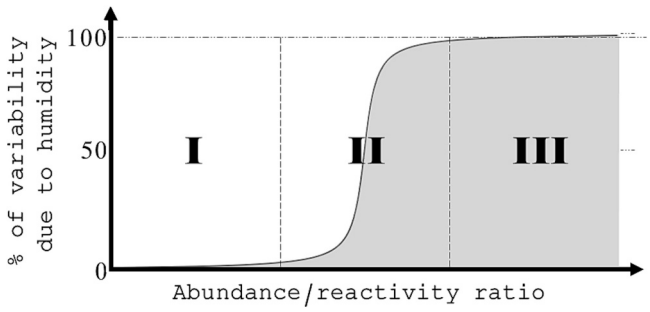

Fig. 1. Conceptual spectrum depicting the relative influence of water vapor on the concentrations, gradients, and diffusive transport of three categories of dry-air gas components. For Category I gases, which are scarce and highly reactive (e.g., ozone), variability driven by humidity fluctuations is negligible. In contrast, the variabilities of Category III gases such as oxygen and noble gases are overwhelmingly governed by changes in humidity because they are inert relative to their abundance. Category II gases with intermediate reactivity, including methane and nitrous oxide, vary due to both their own sources/sinks and those of water vapor.

($\chi_{O_3,d}$) tracks its true fraction (χ_{O_3}) quite approximately, with gradients that provoke diffusion far exceeding the influences of water vapor dynamics. For the other two categories, however, dry-air fractions non-negligibly misrepresent molar fractions and gradients.

Category II gases occupy the spectrum's center and diffuse as a function of source/sink processes involving both water vapor and their own chemical reactions. For example, methanotrophic consumption and geothermal or biological emissions (Knief, 2019) alter methane's surface partial pressures by a few percent (Steele et al., 1987), rivalling humidity's influence; slightly less volatile, nitrous oxide (Singh et al., 1979) is even more likely to diffuse up humidity gradients rather than away from its own sources toward its sinks. By contrast, CO_2 gradients are largely due to its own biochemical sources and sinks; its abundance often varies by dozens of percent (e.g., Brooks et al., 1997), although with non-negligible influence of water vapor.

Oxygen is a Category III gas—one that is abundant and relatively inert, such that variability driven by its own biogeochemical sources and sinks is small compared to humidity-induced dilution of dry air (Supplementary Video S1). Consequently, its molar fractions and gradients are governed primarily by water vapor dynamics. Humidification generates large diffusive fluxes down humidity-driven gradients, but these are nearly offset by opposing non-diffusive mass flow associated with water vapor sources and sinks (Kowalski et al., 2025), so that net transport reflects only the small residual imposed by O_2's own exchanges. Aerobic and oxygenic reactions force p_{O_2} fluctuations of less than 0.01% (Machta and Hughes, 1970). Water vapor that contains neither dry air nor O_2 constitutes up to 5% of tropical air; this implies a χ_d deficit in extremely sultry airmasses of up to 50,000 ppm, of which more than one fifth corresponds to O_2. Thus, χ_{O_2} ranges over 10,000 ppm (1%) and falls below 20% in extremely humid conditions (Fig. 2), dwarfing variations caused by oxygenic and aerobic reactions (error bars in Fig. 2). Sources and sinks of O_2, previously purported to drive variation in air's O_2 content (Keeling and Shertz, 1992), have negligible influence on the overall variability of such a Category III gas.

Humidity's influence on a dry-air constituent's abundance—as well as the gradients that drive its diffusion—are thus negligible for volatile Category I gases but decisive for relatively inert Category III gases like O_2. In the following analyses, we combine χ_d calculated from reanalysis data with well-known and precisely specified information regarding $\chi_{O_2,d}$ to map the global χ_{O_2} distributions that influence aerobic processes and diffusive transport of this Category III gas.

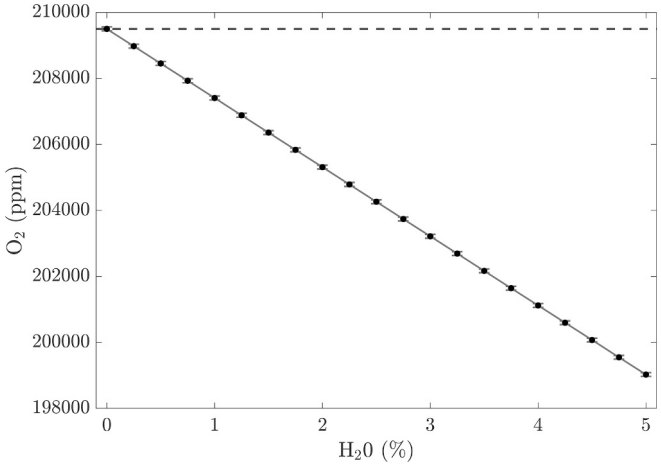

Fig. 2. Molar fractions within moist air: oxygen (O_2; ppm) as a function of water vapor (H_2O; %), based on the assumption that O_2 constitutes 20.946 ± 0.006% of dry air (Machta and Hughes, 1970). Error bars reflect possible deviations of up to ±60 ppm in dry-air O_2 due to biological and oxidation processes. The dashed line indicates previously reported constant O_2 content of air (Keeling and Shertz, 1992).

3. Data and methods

This study estimates χ_d using fifth-generation ECMWF reanalysis for the global climate and weather (ERA5; Hersbach et al., 2020), selected for its continuous, high-resolution atmospheric coverage. The ~31 km spatial resolution and sub-daily frequency enable detailed characterization of surface conditions relevant to O_2 availability, including ensemble-based means and spreads. Retrieved variables include surface pressure (p) and 2-m dewpoint temperature (T_d), along with their ensemble spreads (Δp and ΔT_d), sampled every three hours at native resolution. The vapor pressure (e) was calculated from T_d using Eq. (10) of Bolton (1980) that empirically approximates integration of the Clausius-Clapeyron equation. This allowed quantifying water vapor's molar fraction as:

$$\chi_v = \frac{e}{p}. \tag{3}$$

With this and O_2's dry-air molar fraction taken as $\chi_{O_2,d} = 0.20946$ (Machta and Hughes, 1970), the molar fraction of O_2 was calculated as

$$\chi_{O_2} = (1-\chi_v)\cdot\chi_{O_2,d}, \tag{4}$$

or the product of χ_d (from Eq. (2)) with O_2's proportion within dry air.

We used arithmetic averaging to calculate mean values of p and e (averages denoted as $\bar{p}$ and $\bar{e}$) at each spatial point over different temporal averaging periods. These included individual months of July and January in 1997, to describe seasonal variability, and the entire years of 1997 (strong El Niño event) and 1998 (contrasting La Niña) to characterize interannual fluctuations. The average molar fraction of water vapor is then

$$\overline{\chi_v} = \frac{\bar{e}}{\bar{p}}, \tag{5}$$

and that of O_2 is

$$\overline{\chi_{O_2}} = (1-\overline{\chi_v})\cdot\chi_{O_2,d}. \tag{6}$$

We assessed uncertainties in the three-hour values of χ_{O_2} based on those of its determinants and our calculations' sensitivity to such variability. Uncertainty in $\chi_{O_2,d}$ is taken as $\Delta\chi_{O_2,d} = \pm\, 0.00006$ (Machta and Hughes, 1970). The downloaded ERA5 parameters describing ensemble spread, Δp and ΔT_d, are interpreted as representative of uncertainties in these variables at a given point and instant. Rather than differentiating Eq. (10) of Bolton (1980), we took the Clausius-Clapeyron equation as representing the sensitivity of e to uncertainty in T_d (i.e., $\frac{\partial e}{\partial T_d}$); the product of such sensitivity with ΔT_d yields the vapor pressure uncertainty (Δe).

To characterize propagation of uncertainties, Eq. (3) is differentiated with respect to its dependent variables and multiplied by their uncertainties,

$$\Delta\chi_v = \left|\frac{\partial\chi_v}{\partial e}\right|\cdot\Delta e + \left|\frac{\partial\chi_v}{\partial p}\right|\cdot\Delta p, \tag{7}$$

summing absolute values so as not to assume cancellation of errors from different contributions. The uncertainty in the water vapor molar fraction is thereby defined as

$$\Delta\chi_v = \frac{1}{p}\cdot\Delta e + \frac{e}{p^2}\cdot\Delta p. \tag{8}$$

Similarly differentiating Eq. (4) yields the sensitivity of χ_{O_2} to uncertainties in its determinants, and when multiplying with input uncertainties, this results in

$$\Delta\chi_{O_2} = (1-\chi_v)\cdot\Delta\chi_{O_2,d} + \chi_{O_2,d}\cdot\Delta\chi_v. \tag{9}$$

Because natural variability of time-averaged χ_{O_2} was found to substantially exceed the uncertainties indicated by the ensemble spread, variability was quantified using the standard deviation, which

appropriately reflects the dispersion of atmospheric conditions in this context. This was calculated using weighted statistics, which showed no appreciable difference versus arithmetic statistics. We confirmed that the reanalysis product and ensemble mean yielded very similar results for monthly statistics, and present only the former.

The analysis and figures were carried out with MATLAB v2012b. Additionally, means and standard deviations of p and e over the different temporal averaging periods were calculated using Climate Data Operators (CDO) version 2.0.5.

We downloaded and processed ERA5 monthly mean data for the years 1940–2024 and created a multi-decade, global database of available O_2 that can be accessed at https://zenodo.org/records/17671977.

4. Results

We present primarily distributions of χ_{O_2} because it facilitates comparison with previous reports of air's O_2 content as a simple fraction of dry air ($\chi_{O_2,d}$; Keeling and Shertz, 1992), which was found to be nearly constant and not mapped. At elevation, surface p_{O_2} is greatly reduced—to less than 40% of sea-level atop Mount Everest—and so plotted only for maritime locations to confirm that χ_{O_2} distributions broadly depict available O_2.

4.1. Seasonal snapshots of χ_{O_2}

Oxygen's molar fractions, mapped at 00 UTC during the 1997 solstices and equinoxes (Fig. 3), reveal seasonal distribution trends. Most abundant at the poles, especially the South Pole in winter, O_2 is reduced in tropical humidity. Its gradients are mainly meridional but also vary with season, weather, and surface type. Outside the tropics, especially at boreal latitudes, O_2 is higher in winter—particularly over continents—and lower in summer with stronger zonal gradients.

Subtropical regions show distinct patterns: the Sahara remains O_2-rich year-round, while intermittently sultry regions like India, Southeast Asia, and southeastern North America experience strong seasonal shifts. Intense O_2 gradients appear in the Sahel, Himalayas, and at summer's end along semi-arid coastlines outlining the Red Sea, Persian Gulf, and Mediterranean.

Regional behavior varies widely around the tropics. Low O_2 recurs over the Indian ocean, over archipelagos like Maritime Southeast Asia, and over continents in the Amazon and Congo basins. Regions of high O_2 variability also can be oceanic (American Mediterranean Sea, Bay of Bengal) or terrestrial (Northeast Brazil, tropical Australia).

Generally, zonal gradients persist across seasons in the Atlantic and Pacific, with more aerobic conditions in the east.

4.2. Uncertainties in χ_{O_2}

Globally, uncertainties in the determination of O_2's molar fraction ($\Delta\chi_{O_2}$) are typically much less than 0.1% (1000 ppm; Fig. 4), orders of magnitude smaller than the overestimation errors that occurred when neglecting water vapor (up to 1% or 10,000 ppm, Fig. 2). Exceptionally, $\Delta\chi_{O_2}$ reaches maximum values of order 0.1% in regions characterized by very strong gradients, such as the Sahel (Fig. 4b and c).

The accuracies of our mapped χ_{O_2} distributions depend primarily on the quality of humidity data. Eq. (9) indicates that uncertainties in O_2's molar fraction $(\Delta\chi_{O_2})$ originate from uncertainties in both its dry-air fraction ($\Delta\chi_{O_2,d}$; first term) as well as those of water vapor's molar fraction ($\Delta\chi_v$; second term). Of the errors forced by these two sources, those caused by $\Delta\chi_v$ are greater by an order of magnitude (data not shown).

4.3. Monthly statistics of χ_{O_2}

These seasonal patterns persist in monthly averages, with more consistently meridional gradients (Fig. 5a, b). January features high O_2 at both poles, unlike July when the North Pole is less aerobic. Elevated winter values of O_2 are found in Boreal regions of Asia and North

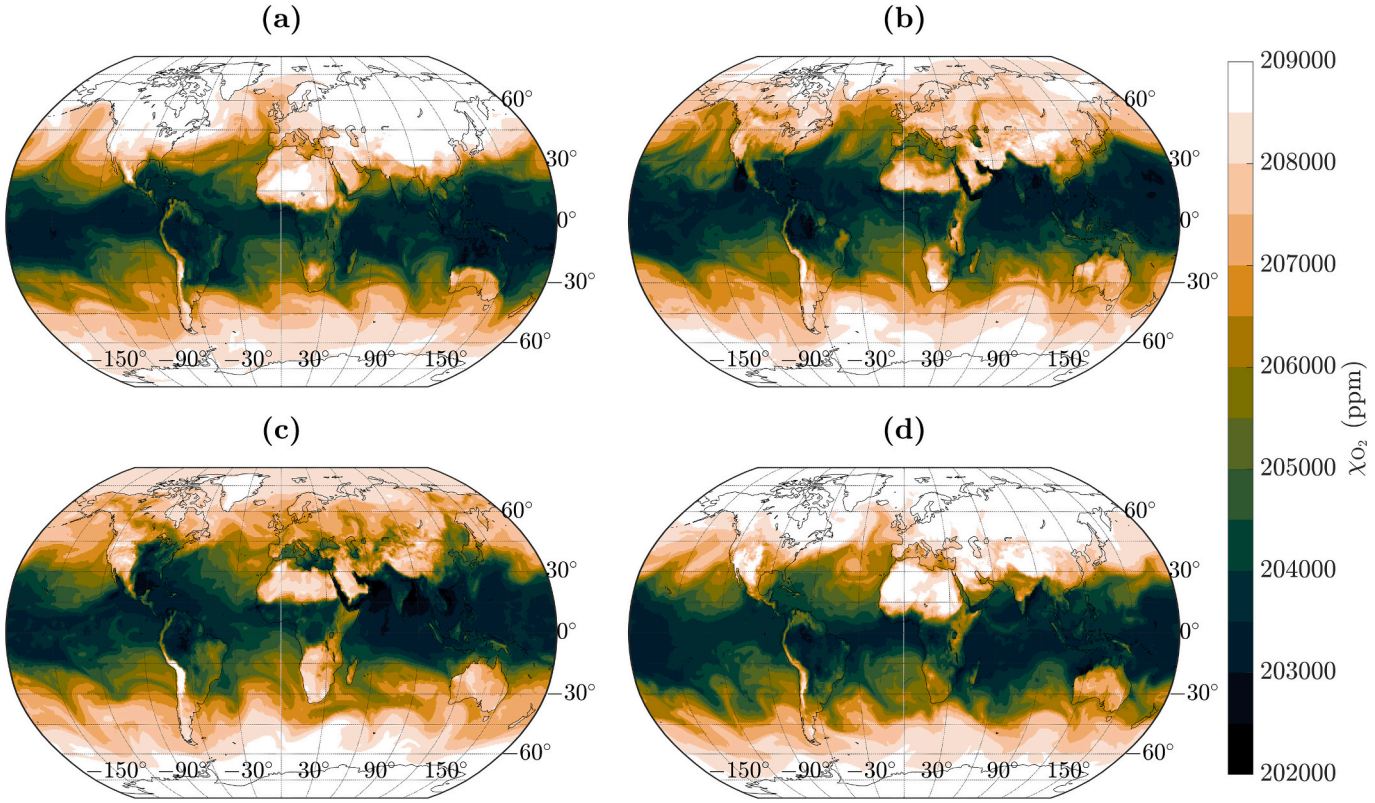

Fig. 3. Snapshots of the molar fraction of oxygen (χ_{O_2}) at 00 UTC for four days of 1997: (a) 21 March; (b) 21 June; (c) 22 September; and (d) 22 December.

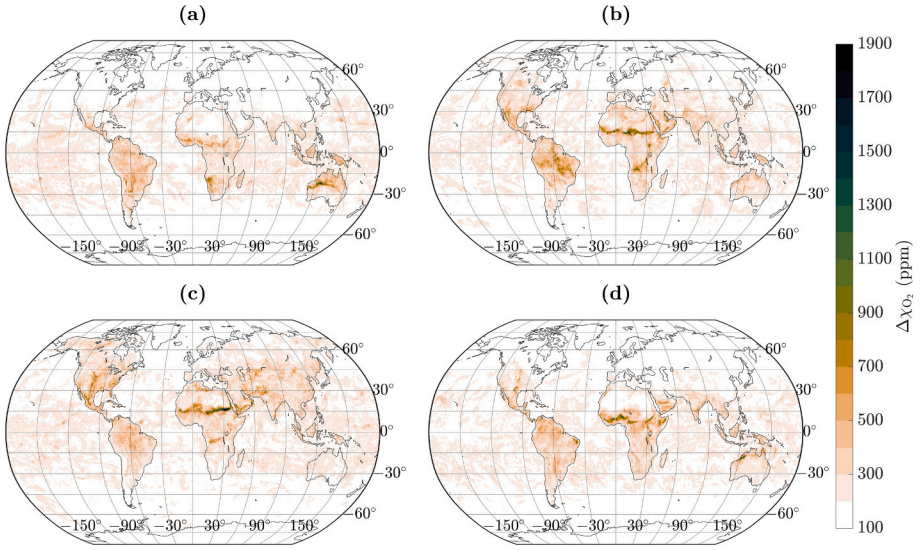

Fig. 4. Uncertainties associated with the molar fraction of oxygen $(\Delta\chi_{O_2})$ at 00 UTC for four days of 1997, as presented in Fig. 3: (a) 21 March; (b) 21 June; (c) 22 September; and (b) 22 December.

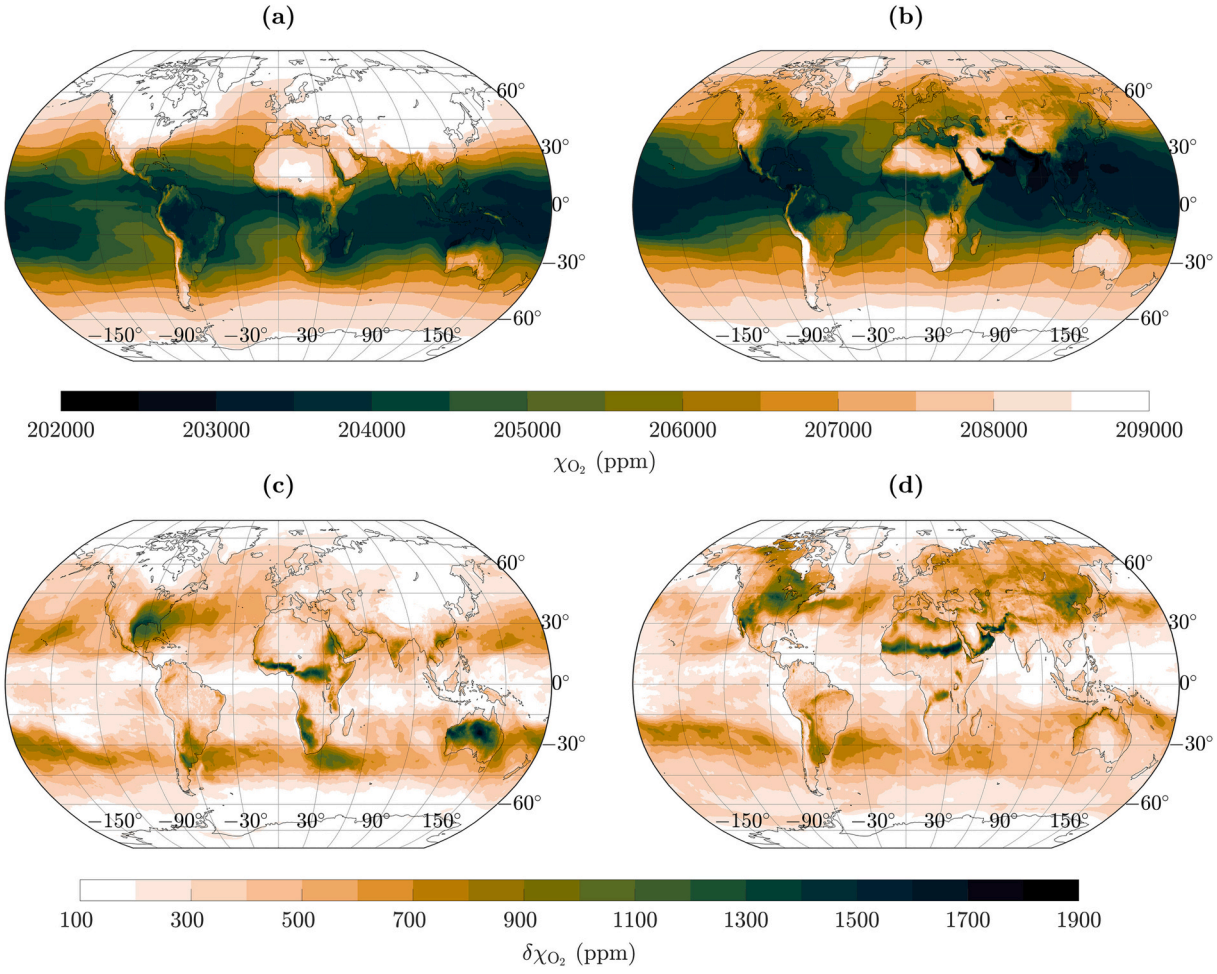

Fig. 5. Averages of molar fraction of oxygen (χ_{O_2}) for the 1997 months (a) January and (b) July, and their standard deviations ($\delta\chi_{O_2}$), also for (c) January and (d) July. Values computed using the ERA5 Reanalysis product.

America, and also the Tibetan Plateau. In Africa, low O_2 areas include the Congo basin year-round, shifting south in January but north in July. Also in July, particularly low O_2 is found in Southern Asia and relatively high O_2 in the Atacama Desert.

Temporal variability within January and July (Fig. 5c, d) is highest in regions with strong O_2 gradients, such as the Sahel—tracking the

Intertropical Convergence Zone's seasonal shift—and the coastlines of the Red Sea (January) and Persian Gulf (July). Notable variability is found in January across Australia, southeastern North America, and southwestern Africa, and in July across much of North America. Globally, O_2 variability is elevated across mid-latitude bands under the influence of storm-tracks (Wallace and Hobbs, 2006).

4.4. Sea-level p_{O_2} and its contrast with previous reports

In broad terms, the sea-level patterns in χ_{O_2} presented above faithfully describe available oxygen (p_{O_2}) and its meridional variation (Fig. 6a and b). Tropical and subtropical zones are relatively hypoxic due to their high humidities, particularly near the coasts of southern Asia, while more aerobic bands occupy temperate zones that expand in winter. However, despite its high values of χ_{O_2}, the subantarctic band near 60° S has relatively low p_{O_2} as a consequence of persistently low p.

The errors that were committed in estimating sea-level p_{O_2} based on dry-air fractions rather than air fractions (i.e., using $\chi_{O_2,d}$ rather than χ_{O_2}; Fig. 6c and d) parallel global distributions of water vapor. These errors (Δp_{O_2}) are negligible in polar winters but exceed 6 hPa over tropical seas and seasonally elsewhere (e.g., the Gulf Stream in July). Since sea-level p_{O_2} is generally of order 210 hPa, they represent relative errors of about 3% in the tropics (equal to χ_v) and are significant regarding the estimation of oceanic O_2 in equilibrium with the atmosphere (via Henry's law).

4.5. Interannual variability

Annually averaged χ_{O_2} values vary most greatly in regions directly affected by the El Niño-Southern Oscillation. The eastern tropical Pacific has higher O_2 during La Niña (1998), whereas Oceania shows greater O_2 during El Niño (1997), as seen when contrasting extreme years (Fig. 7). Yet interannual differences below 0.05% do not significantly alter persistent meridional gradients.

5. Discussion

5.1. Humidity primarily drives atmospheric O_2 variability

Surface O_2 concentrations are greatest wherever and whenever water vapor is scarce, and vice versa, as humidity largely controls the availability of this Category III gas. This contrasts with earlier views based on $\chi_{O_2,d}$, which attributed O_2 variability mainly to its own surface fluxes (Najjar and Keeling, 1997), stoichiometrically coupled to the C cycle. Rather, air's O_2 content is better described by χ_{O_2} and much more strongly influenced by surface fluxes of water vapor, or by the hydrological cycle in general. Previous neglect of water vapor and reliance on $\chi_{O_2,d}$ caused overestimation of O_2 content and great underestimation of its true variability (Fig. 2), which includes regional and seasonal fluctuations over many thousands of ppm (Figs. 3, 5).

Cyclic patterns outside the tropics show summers to be more hypoxic, aligning with non-specialist descriptions of “stifling” summer air

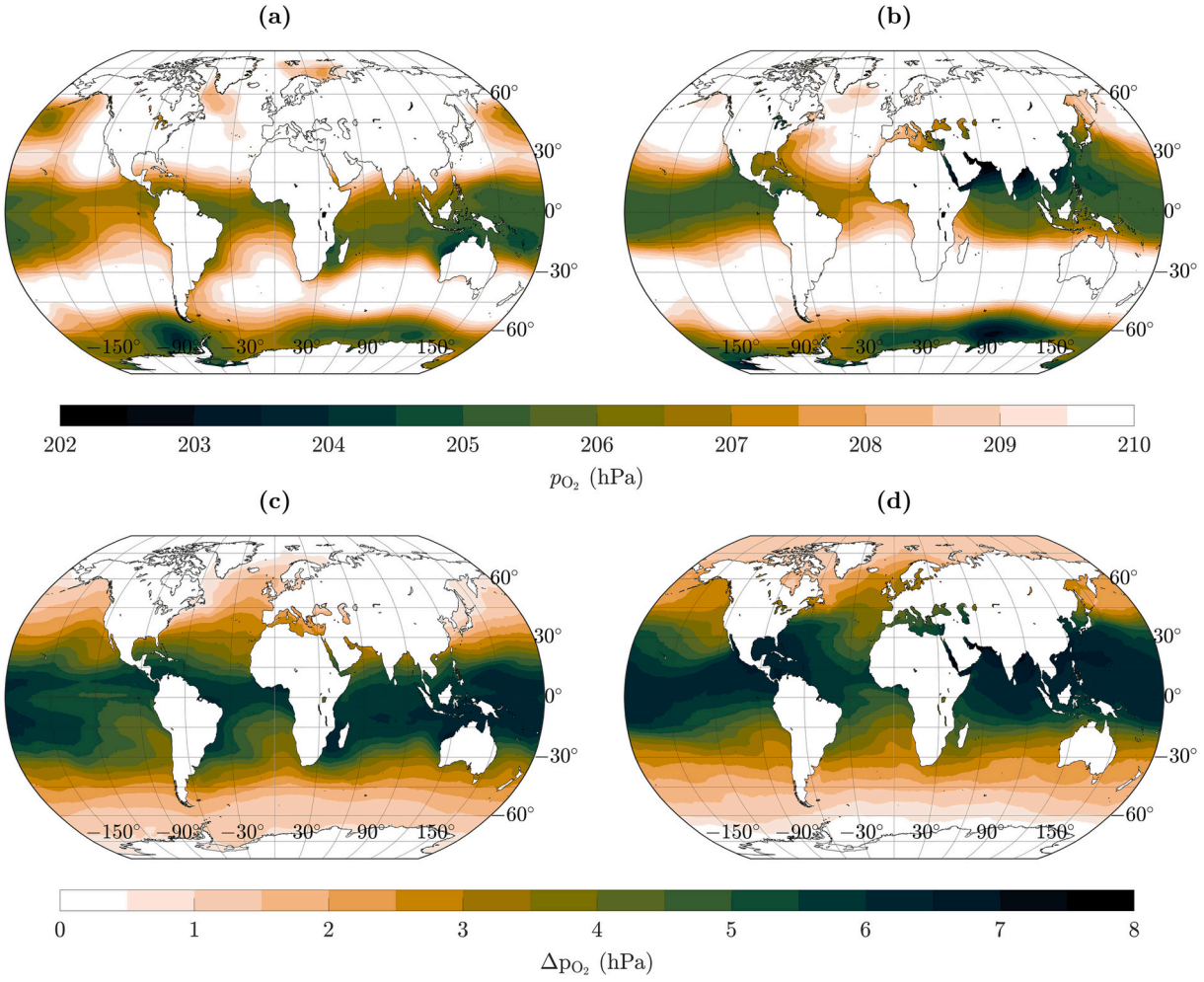

Fig. 6. Sea-level distributions of the partial pressure of oxygen (p_{O_2}) for the 1997 months (a) January and (b) July, and the difference between p_{O_2} calculated when neglecting water vapor and using the dry-air fraction ($\chi_{O_2,d}$), also in (c) January and (d) July.

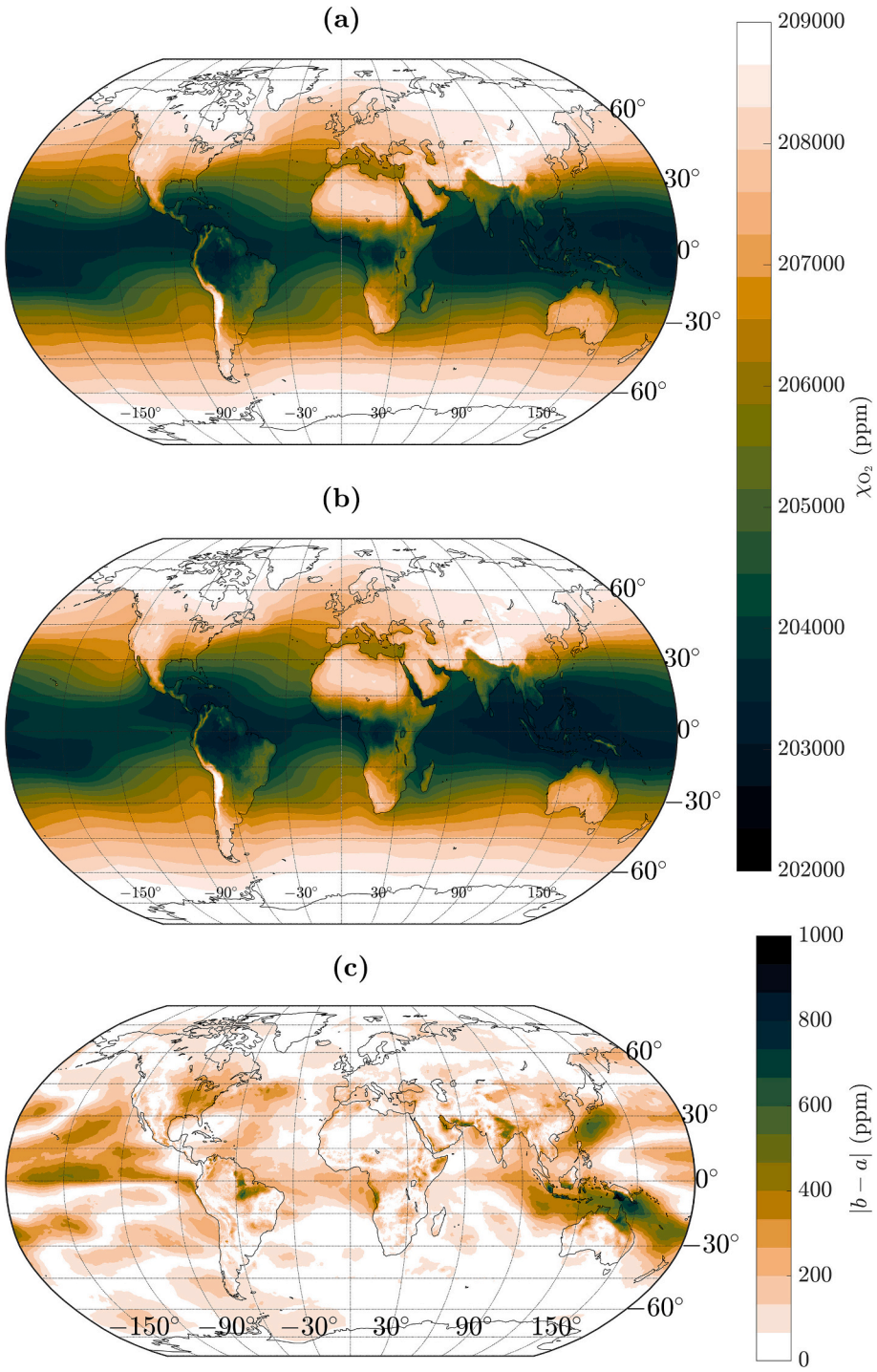

Fig. 7. Averages of the molar fraction of oxygen (χ_{O_2}) for during (a) 1997 (El Niño event) and (b) 1998 (La Niña event) and (c) the absolute value of the difference between the two years.

that complicates breathing (Twain, 1876; Wilde, 1891; see also Camus, 1942), but contradicting earlier reports of high summer O_2 concentrations (Gruber et al., 2001; Petsch, 2003). In either hemisphere, extratropical evapotranspiration suppresses O_2 in summer by hundreds or thousands of ppm, in contrast to interpretations based on $\chi_{O_2,d}$ that purported summer *elevation* of O_2 by dozens of ppm (Keeling et al., 1993). The notion that hemispheric O_2 variations mirror those of CO_2 and imply minimal cross-equatorial exchange (Gruber et al., 2001; Keeling et al., 1998) overlooks massive seasonal shifts in water vapor and dry air (including O_2). Unlike CO_2, a Category II gas driven predominantly by photosynthesis and respiration, O_2 is a Category III gas overwhelmingly controlled by the hydrological cycle. Although biochemically linked, O_2 and CO_2 differ greatly regarding the determinants of their atmospheric distributions and therefore transport mechanisms.

Interpretations based on $\chi_{O_2,d}$ similarly failed to notice largescale atmospheric O_2 gradients (Keeling et al., 1993), which are primarily poleward, greatly informative regarding the principal mechanism of atmospheric O_2 transport and exert physical control over air-sea O_2 exchanges as described below.

5.2. Regional gradients and implications regarding transport

Regional O_2 availability reflects meteorological controls operating across multiple scales, as illustrated by several emblematic environments. Subtropical deserts such as the Sahara are strongly aerobic: synoptic- to regional-scale subsidence imports dry air toward the surface, while microscale transport of evaporated water vapor—governed by surface-layer turbulence—is weak due to low evaporation. In contrast, the Western Pacific Warm Pool is persistently hypoxic, owing to intense evaporation combined with large-scale atmospheric ascent. High-altitude regions such as the Tibetan Plateau differ for entirely separate reasons, remaining relatively oxygenated in winter primarily due to cold, dry mountain meteorology.

A tropical rainforest like the Amazon reduces O_2 concentrations by thousands of ppm (Figs. 3, 5, 6) via intense evapotranspiration (Miralles et al., 2011), despite being a net O_2 producer (Malhi et al., 2021). Even during daytime, water vapor's evaporative source overwhelms the modest photosynthetic O_2 increases (Kowalski, 2025) registered by $\chi_{O_2,d}$ (Keeling and Shertz, 1992) to curtail the availability of this Category III gas. Such humid suppression dominates χ_{O_2} variability in the tropics and subtropics, making atmospheric O_2 far less abundant than previously reported when water vapor was neglected. Only in cold, arid environments where humidity is minimal—such as polar winters or the upper atmosphere—do older estimates remain valid, though such regions have limited biochemical impact.

Oxygen distributions provide key insight into atmospheric transport mechanisms. Across biological scales—from leaf to biome—approaching transpiring vegetation corresponds to increasing hypoxia. Leaf emissions are more than 99% water vapor; their mere trace O_2 dilutes ambient air containing more than one-fifth O_2. This evaporative dilution is strongest in tropical rainforests (Figs. 3, 5, 6; Miralles et al., 2011), regions that nonetheless export O_2 (Malhi et al., 2021), implying up-gradient, non-diffusive transport. Oxygen diffuses *toward* evaporating surfaces—even those with net O_2 emissions (Yan et al., 2023)—since humidification suppresses Category III gas concentrations. Yet net O_2 transport is in the opposite direction. As seen from leaf pores (Kowalski, 2025) to boundary-layer flows (Kowalski et al., 2021), evapotranspiration both dilutes and displaces dry air, activating diffusive and non-diffusive mechanisms with the latter dominating net O_2 transport. These hydrologically driven airflows extend to the global scale, as described next.

Recognition of net, meridional mass flow of the atmosphere follows from two key principles: (1) the hydrological cycle transports water vapor poleward (Zhang et al., 2013); and (2) water vapor overwhelmingly dominates dry-air components in terms of air's sources and sinks that drive fluxes (Kowalski, 2017). As a result, the average poleward momentum of the atmosphere matches that of water vapor, much like how evapotranspiration drives airflows out of stomata (Kowalski, 2017, 2025) and upward in the atmospheric boundary layer (Kowalski, 2017; Kowalski et al., 2021), enabling up-gradient O_2 transport in each case. At the global scale, meridional flow conveys every air constituent, including O_2, away from the tropics. The return leg of the hydrological cycle—in liquid phase—has no direct impact on atmospheric transport. Meanwhile, dry air (and thus O_2) diffuses equatorward, opposing water vapor diffusion. For inert Category III gases like argon, these opposing mechanisms nullify, resulting in no net meridional transport.

Influential research based on atmospheric gas transport has generally conflated diffusive and non-diffusive mechanisms. For example, top-down approaches (atmospheric inversions) to assess sources and sinks of greenhouse gases generally assume that they diffuse according to gradients in their dry-air fractions (Masarie and Tans, 1995; Bousquet et al., 1999; Tian et al., 2016). The consequences of neglecting how water vapor dynamics actuates both diffusive and non-diffusive transport of other gases may be worthy of investigation in this context.

5.3. Implications for atmospheric exchanges with oceans

These O_2 distributions challenge existing ocean-atmosphere cycling theories. Henry's law states that a gas's dissolution is directly proportional to its partial pressure. The previous neglect of humidity's control over χ_{O_2} and p_{O_2} (Keeling and Shertz, 1992) was foundational to defining the dissolved ocean's O_2 anomaly (Najjar and Keeling, 1997) and to developing ocean biogeochemical models (Aumont et al., 2015), each based on the supposed constancy of O_2 (inferred from $\chi_{O_2,d}$). Seasonal changes in O_2 availability as reflected by the variability of χ_{O_2} help explain oceanic outgassing in summer and ingassing in winter—previously attributed solely to thermal and biological factors (Portela et al., 2024)—and thereby influence meridional transport of oceanic O_2.

5.4. Does χ_{O_2} or p_{O_2} better describe available O_2?

The influence of ambient p on available O_2—whether through sub-antarctic differences between Figs. 5 and 6 or with increasing altitude—is subtle and demands careful treatment. It is accepted that p_{O_2} is the gas-phase determinant both of dissolution via Henry's law and of oxygenic reactions like respiration (Forrer et al., 2023), combustion (Dollwig et al., 1917) and other oxidation reactions (Milena-Pérez et al., 2023). Yet ambient availability does not necessarily reflect conditions at the site of consumption, where O_2 is locally depleted and often depends on replenishment by molecular diffusion. Although a drop in total p lowers all gas partial pressures (including p_{O_2}) it counteractingly lengthens molecular mean free paths and enhances diffusivities. In theory, these opposing effects can offset such that gas availability at the site of consumption is invariant to changes in p (Gale, 1972). In such cases, χ_{O_2} may better represent available O_2 than p_{O_2}.

5.5. Available O_2 in biogeochemical environments

Humid suppression, beyond its global effect on ambient O_2 availability, strongly influences aerobic processes in certain microenvironments. This is particularly evident over extensive evaporating surfaces that substantially humidify the surrounding air. Beneath land surfaces, shallow soils can exceed 40 °C while maintaining near saturation (e.g., Li et al., 2026), implying high values of e that render soil pores relatively hypoxic and may constrain organic matter mineralization (Keiluweit et al., 2016). Over the ocean, evaporation occurs when near-surface e is lower than its saturation value ($e < e_s$) producing negative vertical vapor pressure gradients ($\frac{\partial e}{\partial z} < 0$). As a result, air adjacent to the surface attains high e, suppressing O_2 availability for dissolution in seawater.

6. Conclusions

We have presented the first comprehensive and physically consistent distributions of atmospheric O_2 near the Earth's surface that explicitly account for the controlling influence of humidity. Contrary to the previously assumed constant value of 20.946 ± 0.006%, air's O_2 content is both lower and considerably more variable than has traditionally been reported. Substantial O_2 reductions are observed in tropical environments, depressed by as much as 10,000 ppm under extreme humidity, versus the O_2 fraction within dry air. Certain extratropical regions also experience markedly reduced O_2 levels during sultry periods. Our calculated O_2 concentrations are accurate to better than ±1000 ppm, despite having merely bounded the influence of aerobic consumption and oxygenic processes; this can be improved in the future by direct measurement of O_2 in dry air while precisely accounting for eliminated water vapor. These distributions make clear that the predominant mechanism of O_2 transport is not diffusive.

Because O_2 constitutes a major component of air (generally above 200,000 ppm), the discrepancy between its molar fraction in air and that in dry air is substantial, particularly in comparison to greenhouse gases.

However, it is also true of some greenhouse gases that discarded matter should be quantified whenever eliminating a constituent before analyzing air composition, as analytical methods may require regarding humidity. Otherwise, erroneous conclusions may be drawn regarding their gradients and diffusion.

CRediT authorship contribution statement

Andrew S. Kowalski: Writing – review & editing, Writing – original draft, Conceptualization. **Matilde García-Valdecasas Ojeda:** Writing – review & editing, Software, Data curation.

Declaration of Generative AI and AI-assisted technologies in the writing process

During the preparation of this work the authors used ChatGPT in order to improve paragraph concision and tone. After using this tool/service, the authors reviewed and edited the content as needed and take full responsibility for the content of the published article.

Declaration of competing interest

The authors declare that they have no known competing financial interests or personal relationships that could have appeared to influence the work reported in this paper.

Data availability

The codes to calculate the oxygen molar fraction and generate the figures in this study (García-Valdecasas Ojeda and Kowalski, 2025) are available in a Zenodo repository at https://zenodo.org/records/17671977. Additionally, a global dataset of oxygen concentration and partial pressure is available from 1940 to 2024, which was derived from ERA5 monthly mean data (https://cds.climate.copernicus.eu/datasets/reanalysis-era5-single-levels-monthly-means?tab=download).

Acknowledgments

ASK was supported by the project PID2024-158786NB-C21, financed by MICIU/AEI/10.13039/501100011033. MGVO was funded by the project PID2021-126401OB-I00, financed by MICIU/AEI/10.13039/501100011033 and by FEDER. Helpful reviewer suggestions improved this manuscript.

Appendix A. Supplementary data

Supplementary data to this article can be found online at https://doi.org/10.1016/j.scitotenv.2026.181809.

References

Aumont, O., et al., 2015. PISCES-v2: an ocean biogeochemical model for carbon and ecosystem studies. Geosci. Model Dev. 8, 2465–2513. https://doi.org/10.5194/gmd-8-2465-2015.
Bolton, D., 1980. The computation of equivalent potential temperature. Monthly Weather Rev. 108, 1046–1053.
Bousquet, P., et al., 1999. Inverse modelling of annual atmospheric CO2 sources and sinks 1. method and control inversion. J. Geophy. Res.: Atmos. 104, 26161–26178.
Brooks, J.R., et al., 1997. Vertical gradients in photosynthetic gas exchange characteristics and refixation of respired CO_2 within boreal forest canopies. Tree Physiol. 17, 1–12.
Camus, A., 1942. L'étranger. Gallimard, Paris.
Dai, A., 2006. Recent climatology, variability, and trends in global surface humidity. J. Climate 19, 3589–3606. https://doi.org/10.1175/JCLI3816.1.
Dollwig, H.C., et al., 1917. Some observations on the effect of the partial pressure of oxygen on combustion. J. Am. Chem. Soc. 39, 2224–2231.
Famiglietti, C.A., et al., 2018. Global validation of MODIS near-surface air and dew point temperatures. Geophys. Res. Lett. 45, 7772–7780. https://doi.org/10.1029/2018GL077813.
Forrer, A., et al., 2023. Partial pressure of arterial oxygen in healthy adults at high altitudes: a systematic review and meta-analysis. JAMA Netw. Open 6 (6), e2318036. https://doi.org/10.1001/jamanetworkopen.2023.18036.
Gale, J., 1972. Availability of carbon dioxide for photosynthesis at high altitudes: theoretical considerations. Ecology 149, 78–90.
García-Valdecasas Ojeda, M., Kowalski, A.S., 2025. Data and code for "humidity-determined distributions of surface oxygen" [data set]. Zenodo. https://zenodo.org/records/17671977.
Gruber, N.M., et al., 2001. Air-sea flux of oxygen estimated from bulk data: implications for the marine and atmospheric oxygen cycles. Glob. Biogeochem. Cycles 15 (4), 783–803. https://doi.org/10.1029/2000GB001302.
Hersbach, H., et al., 2020. The ERA5 global reanalysis. Q. J. R. Meteorol. Soc. 146, 1999–2049. https://doi.org/10.1002/qj.3803.
Keeling, R.F., Shertz, S.R., 1992. Seasonal and interannual variations in atmospheric oxygen and implications for the global carbon cycle. Nature 358, 723–717.
Keeling, R.F., et al., 1993. What atmospheric oxygen measurements can tell us about the global carbon cycle. Glob. Biogeochem. Cycles 7, 37–67. https://doi.org/10.1029/92GB02733.
Keeling, R.F., et al., 1998. Seasonal variations in the atmospheric O2/N2 ratio in relation to the kinetics of air-sea gas exchange. Glob. Biogeochem. Cycles 12, 141–163. https://doi.org/10.1029/97GB02339.
Keiluweit, M., et al., 2016. Are oxygen limitations under recognized regulators of organic carbon turnover in upland soils? Biogeochem. 127, 157–171.
Khalil, M.A.K., et al., 2002. Atmospheric nitrous oxide: patterns of global change during recent decades and centuries. Chemosphere 47, 807–821. https://doi.org/10.1016/S0045-6535(01)00297-1.
Knief, C., 2019. Diversity of methane cycling microorganisms in soils and their relation to oxygen. Curr. Issues Mol. Biol. 33, 23–56. https://doi.org/10.21775/cimb.033.023.
Kowalski, A.S., 2017. The boundary condition for vertical velocity and its interdependence with surface gas exchange. Atmos. Chem. Phys. 17, 8177–8187. https://acp.copernicus.org/articles/17/8177/2017.
Kowalski, A.S., 2025. An elucidatory model of oxygens partial pressure inside substomatal cavities. Biogeosci 22, 785–789. https://doi.org/10.5194/bg-22-785-2025.
Kowalski, A.S., et al., 2021. Disentangling turbulent gas diffusion from non-diffusive transport in the boundary layer. Boundary-Layer Meteorol. 179 (3), 347–367.
Kowalski, A.S., et al., 2025. Water vapour dynamics as a key determinant of atmospheric composition and transport mechanisms. Biogeosciences 22 (24), 8005–8012. https://bg.copernicus.org/articles/22/8005/2025/.
Li, R., Feng, H., Xue, Y., Zhou, J., Fang, L., Su, D., Zheng, X., Tan, S., Zheng, H., Ma, Y., 2026. Soil water vapor adsorption and condensation governed by groundwater depth and vadose zone lithology in arid and semi-arid regions. J. Hydrol. 670, 135137. https://doi.org/10.1016/j.jhydrol.2026.135137.
Machta, L., Hughes, E., 1970. Atmospheric oxygen in 1967 to 1970. Science 168, 1582–1584.
Malhi, Y., et al., 2021. Biogeochemical cycles of the Amazon. In: Nobre, C., et al. (Eds.), Amazon Assessment Report 2021. United Nations Sustainable Development Solutions Network, New York.
Masarie, K.A., Tans, P.P., 1995. Extension and integration of atmospheric carbon dioxide data into a globally consistent measurement record. J. Geophy. Res.: Atmos. 100 (D6), 11593–11610.
Milena-Pérez, A., et al., 2023. Exploring the impact of temperature and oxygen partial pressure on the spent nuclear fuel oxidation during its dry management. Sci. Rep. 13, 1966. https://doi.org/10.1038/s41598-023-29265-w.
Miralles, D.G., et al., 2011. Magnitude and variability of land evaporation and its components at the global scale. Hydrol. Earth Syst. Sci. 15, 967–981. https://hess.copernicus.org/articles/15/967/2011/hess-15-967-2011.html.
Najjar, R.G., Keeling, R.F., 1997. Analysis of the mean annual cycle of the dissolved oxygen anomaly in the World Ocean. J. Mar. Res. 55, 117–151.
Najjar, R.G., Keeling, R.F., 2000. Mean annual cycle of the air-sea oxygen flux: a global view. Global Biogeochem. Cycles 14 (2), 573–584. https://doi.org/10.1029/1999GB900086.
Novelli, P.C., et al., 1999. Molecular hydrogen in the troposphere: global distribution and budget. J. Geophys. Res. 104 (D23), 30427–30444. https://doi.org/10.1029/1999JD900788.
Owen, J.M, Pincombe, J.R., Rogers, R.H., 1985. Source-sink flow inside a rotating cylindrical cavity. J. Fluid Mech. 155, 233–265.
Pérez-Priego, O., et al., 2015. Analysing uncertainties in the calculation of fluxes using whole-plant chambers: random and systematic errors. Plant Soil 393 (1), 229–244. https://doi.org/10.1007/s11104-015-2481-x.
Petsch, S.T., 2003. The global oxygen cycle. In: Schlesinger, W., et al. (Eds.), Treatise on Geochemistry Volume 8. Elsevier, Amsterdam.
Portela, E., et al., 2024. The Ocean's meridional oxygen transport. J. Geophys. Res. Oceans 129, e2023JC020259. https://doi.org/10.1029/2023JC020259.
Prinn, R., et al., 1990. Atmospheric emissions and trends of nitrous oxide deduced from 10 years of ALE-GAGE data. J. Geophys. Res. Atmos. 95, 18369–18385. https://doi.org/10.1029/JD095iD11p18369.
Raich, J.W., Schlesinger, W.H., 1992. The global carbon dioxide flux in soil respiration and its relation to vegetation and climate. Tellus 44B, 81–99.
Robeson, S.M., Steyn, D.G., 1990. Evaluation and comparison of statistical forecast models for daily maximum ozone concentrations. Atmos. Env. 24, 303–312. https://doi.org/10.1016/0957-1272(90)90036-T.
Singh, H.B., et al., 1979. The distribution of nitrous oxide (N2O) in the global atmosphere and the Pacific Ocean. Tellus 31A, 313–320. https://doi.org/10.3402/tellusa.v31i4.10439.

Spelce, D., et al., 2016. Respiratory protection for oxygen deficient atmospheres. J. Int. Soc. Respir. Prot. 33 (2), 32336876.
Steele, L.P., et al., 1987. The global distribution of methane in the troposphere. J. Atmos. Chem. 5, 125–171.
Tian, H., et al., 2016. The terrestrial biosphere as a net source of greenhouse gases to the atmosphere. Nature 531, 225–228. https://doi.org/10.1038/nature16946.
Tohjima, Y., et al., 2005. Preparation of gravimetric standards for measurements of atmospheric oxygen and reevaluation of atmospheric oxygen concentration. J. Geophys. Res. Atmos. 110, D11302. https://doi.org/10.1029/2004JD005595.
Twain, M., 1876. The Adventures of tom Sawyer. The American Publishing Company, Cincinnati, OH.
Wallace, J.M., Hobbs, P.V., 2006. Atmospheric Science: An Introductory Survey. Elsevier, Amsterdam.
Watson, A., et al., 1978. Methanogenesis, fires and the regulation of atmospheric oxygen. BioSystems 10, 293–298.
Wilde, O., 1891. The Picture of Dorian Gray. Simpkin, Marshall, Hamilton, Kent and Co., London.
Yan, Y., et al., 2023. A modeling approach to investigate drivers, variability and uncertainties in O2 fluxes and O2: CO2 exchange ratios in a temperate forest. Biogeosciences 20, 4087–4107. https://doi.org/10.5194/bg-20-4087-2023.
Zhang, X., et al., 2013. Enhanced poleward moisture transport and amplified northern high-latitude wetting trend. Nat. Clim. Chang. 3, 47–51. https://doi.org/10.1038/nclimate1631.